Journal of Alloys and Compounds 688 (2016) 1095–1100

Contents lists available at ScienceDirect

Journal of Alloys and Compounds

journal homepage: http://www.elsevier.com/locate/jalcom

# Magnetic, transport, and magnetotransport properties of the textured $Fe_3O_4$ thin films reactively deposited onto $SiO_2$/Si

A.S. Tarasov [a, b, *], M.V. Rautskii [a], A.V. Lukyanenko [a, b], M.N. Volochaev [a, c], E.V. Eremin [a, b, c], V.V. Korobtsov [d, e], V.V. Balashev [d, e], V.A. Vikulov [d], L.A. Solovyov [f], N.V. Volkov [a, b]

[a] Kirensky Institute of Physics, Russian Academy of Sciences, Siberian Branch, Krasnoyarsk, 660036, Russia
[b] Institute of Engineering Physics and Radio Electronics, Siberian Federal University, Krasnoyarsk, 660041, Russia
[c] Siberian State Aerospace University, Krasnoyarsk, 660014, Russia
[d] Institute of Automation and Control Processes, Russian Academy of Sciences, Far Eastern Branch, Vladivostok, 690041, Russia
[e] School of Natural Sciences, Far Eastern Federal University, Vladivostok, 690922, Russia
[f] Institute of Chemistry and Chemical Technology, Russian Academy of Sciences, Siberian Branch, Krasnoyarsk, 660049, Russia

ARTICLE INFO

*Article history:*
Received 24 November 2015
Received in revised form
27 May 2016
Accepted 14 July 2016
Available online 16 July 2016

*Keywords:*
Magnetite
Magnetoresistance
Reactive deposition

ABSTRACT

The structural, magnetic, transport, and magnetotransport properties of $Fe_3O_4$ thin films with thicknesses from 38 nm to 95 nm are systematically investigated. The occurrence of the Verwey transition in these films at a temperature of about 120 K is established. It is found that the temperature dependences of the magnetic moment have a feature near 40 K, which can be attributed to the multiferroic phase. According to the X-ray diffraction data, the film structure represents a (001) texture. As was established using transmission electron microscopy, the height and width of texture crystallites increase with film thickness. Analysis of the temperature dependences of the resistivity showed that the dominant carrier transport mechanism in the films is thermoactivated tunneling. The thermoactivation energy, along with the room-temperature resistivity, decreases with increasing film thicknesses, which is most likely related to the variation in the crystallite size, especially in the crystallite width. The field dependence of magnetoresistance behaves similarly over the entire temperature range and has a positive MR peak in weak fields, which is related to spin-dependent tunneling through $Fe_3O_4$ grains and antiferromagnetically coupled antiphase boundaries.



## 1. Introduction

Magnetite ($Fe_3O_4$) is a well-known magnetic material with a Neel temperature of $T_N$ = 860 K and the cubic inverse spinel structure, in which $Fe^{3+}$ ions occupy the tetrahedral A sites and octahedral B sites and $Fe^{2+}$ ions, only the octahedral B sites. Magnetite is a ferrimagnet, since the magnetic moments of iron ions in the A and B sites are antiparallel and uncompensated. Since at high temperatures $Fe^{2+}$ and $Fe^{3+}$ ions are dynamically distributed over the crystal, the resistivity of magnetite is relatively low due to hopping conductivity between $Fe^{2+}$ and $Fe^{3+}$ ions. Below 120 K, the resistivity sharply increases due to the charge ordering of $Fe^{2+}$ and $Fe^{3+}$ ions, which is accompanied by the crystal symmetry change from the cubic inverse spinel $Fd\bar{3}m$ to noncentrosymmetric monoclinic *Cc*; i.e., the Verwey transition occurs [1–3]. However, the Verwey charge ordering hypothesis [1] is correct to the first approximation. As was shown in recent works [4,5], electrons are not completely localized, but distributed over three B sites with the formation of a charge density wave along the infinite B chain. One more transition of unclear origin is observed below 40 K. According to the experimental data reported in Refs. [6,7], below 40 K magnetite exhibits the multiferroic properties.

In addition, magnetite is interesting for application in spintronic devices, since it has the extremely high (~80% [8–10]) degree of spin polarization of conduction electrons and high $T_N$. Magnetite can be epitaxially grown on semiconductor substrates with a sublayer [11]. Moreover, the electrical spin injection into GaAs by a magnetite spin injector has recently been demonstrated [12]. In

* Corresponding author. Kirensky Institute of Physics, Russian Academy of Sciences, Siberian Branch, Krasnoyarsk, 660036, Russia.
*E-mail address:* taras@iph.krasn.ru (A.S. Tarasov).

http://dx.doi.org/10.1016/j.jallcom.2016.07.138
0925-8388/

view of this, the attention of researches has been focused upon the transport and magnetotransport properties of the magnetite films [13–17] and multilayered structures [18–20]. It was shown that the magnetoresistance (MR) of magnetite can be negative in epitaxial [13] and polycrystalline films [14], positive in weak magnetic fields and negative in strong magnetic fields; i.e., the MR in epitaxial films changes its sign with increasing magnetic field [15–17]. These effects are attributed to the antiferromagnetically coupled antiphase boundaries (AF APBs) and structural defects, which are formed in the {110} planes and characterized by the (1/4)a[110] crystal translation [21]. In this case, antiferromagnetic ordering is established at the interface between two ferrimagnetic regions. The formation of such defects underlies the occurrence of the anomalous magnetoresistance.

The aim of this study was to investigate the structural, magnetic, transport, and magnetotransport properties of textured $Fe_3O_4$ thin films of different thicknesses reactively deposited onto Si wafers. Magnetic field dependences of MR behave similarly over the entire temperature range and contain a positive MR peak in weak fields. The observed MR effect is attributed to spin-dependent tunneling across $Fe_3O_4$ grains and AF APBs, whose concentration in the prepared textured $Fe_3O_4$ (001) films can be sufficiently high.

## 2. Experimental

$Fe_3O_4$ thin films with thicknesses from 38 to 95 nm were synthesized by reactive deposition of Fe onto the $SiO_2$/Si(001) surface in the $O_2$ atmosphere at a substrate temperature of 300 °C. The experiments were carried out in an ultra-high vacuum MBE system equipped with a 20-keV reflection high-energy electron diffraction (RHEED) and spectral ellipsometry tools. During deposition, the partial molecular oxygen gas pressure was kept constant at a level of about $3 \times 10^{-6}$ Torr. Iron was thermally evaporated from an alumina crucible at a rate of 2.5 nm/min. The *n*-Si(001) wafers with a doping density of $N_D = 6\times10^{14}$ cm$^{-3}$ (resistivity of 7 Ω cm) were used as substrates. Before loading into a vacuum chamber, the Si(001) substrates were coated with an ultrathin (~1.5 nm) $SiO_2$ layer grown by boiling the Si substrate in nitric acid for 5 min.

X-ray diffraction (XRD) investigations were carried out on a PANalytical X'Pert Pro MPD diffractometer with a PIXcel high-speed detector and graphite monochromator (CuKα radiation) in the angular range of 28–60° 2Θ. The degree of preferred orientation and cubic lattice parameter were determined by the full-profile derivative difference minimization (DDM) method [22]. In addition, the film structure was studied by atomic force microscopy (AFM) and cross-sectional transmission electron microscopy (TEM). The magnetic properties were studied on a PPMS-9 Physical Property Measurement System. Ferromagnetic resonance (FMR) spectra were measured using a Bruker ELEXSYS E580 system in the X band (9.45 GHz). Resistivity and MR were measured in the four-probe configuration on an original facility comprising a helium cryostat, an electromagnet, and a Keithley's-2400 precision current/voltage source meter.

## 3. Results and discussion

### 3.1. Structural characterization

Fig. 1a shows an XRD pattern of the 55-nm-thick $Fe_3O_4$ film. The absence of any peaks, except for the $Fe_3O_4$ reflections, indicates that the film contains no impurities or foreign phases. The full-profile DDM refinement of the XRD pattern revealed the best agreement between the observed and calculated diffraction intensities for a model of preferred orientation of the $Fe_3O_4$ crystallographic plane (001) with an orientation degree of 30%. The calculated lattice constant is 8.398(6) Å, which is consistent with the lattice constant of the bulk crystal (8.396 Å) within the experimental error [23].

Fig. 1b shows an AFM image of the sample surface. One can clearly see grains about 70 nm in size. This surface morphology characterizes all the investigated films. To analyze the films microstructure in more detail, we carried out TEM investigations. Cross-sectional TEM images of the $Fe_3O_4/SiO_2$/n-Si structures are presented in Fig. 2. The dark-field TEM image was obtained for (311) and (222) $Fe_3O_4$. First, one can see the film of uniform thickness with crystallites of nearly the same height (Fig. 2a and b). Second, under stronger magnification, the atomic planes of the $Fe_3O_4$ crystal and the $SiO_2$ layer can be clearly seen (Fig. 2c and d). Third, the height and width of crystallites increase with film thickness (Fig. 2d–g). This correlation, however, can be followed only until the thickness of 55 nm; as the thickness increases from 55 to 95 nm, the crystallite width does not proportionally grow. These details were not revealed by AFM study, probably, because of the cantilever curvature radius of ~20 nm.

### 3.2. Magnetic properties

The magnetic properties were measured in a magnetic field parallel to the film plane. Zero-field-cooling (ZFC) and field-cooling

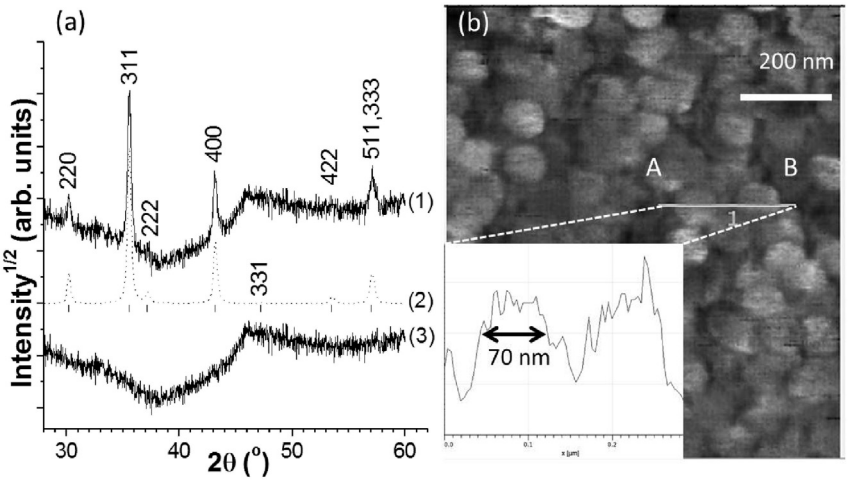


**Fig. 1.** XRD and AFM images of the 55-nm-thick $Fe_3O_4$ film on the Si(001) wafer. (a) XRD patterns after full-profile DDM refinement. (1) Observed, (2) calculated, and (3) difference profiles, reflection positions and indices. (b) AFM image and cross-sectional profile for two grains.

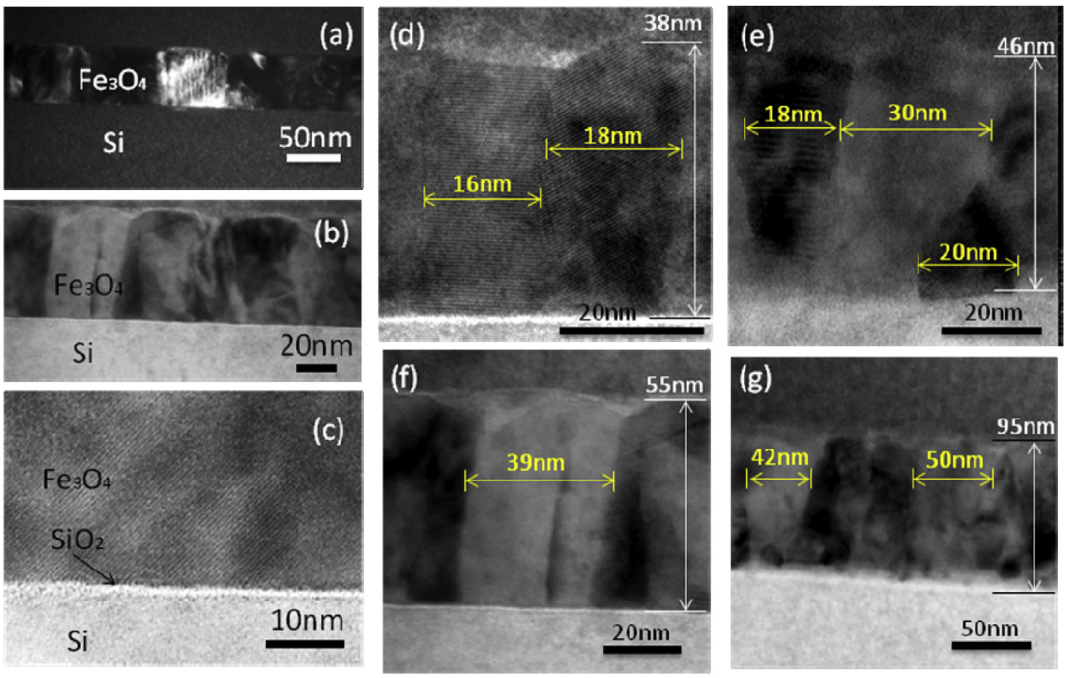


**Fig. 2.** (a) Dark- and (b, c) bright-field cross-sectional TEM images of the $Fe_3O_4$(55 nm)/$SiO_2$/n-Si structure at different magnifications. (d–g) Images of the films with thicknesses of 38, 46, 55, and 95 nm.

(FC) curves M(T) were obtained in a magnetic field of 2 kOe (Fig. 3). First, we observe a sharp decrease in the magnetic moment upon cooling, which is indicative of the occurrence of the Verwey transition [1] caused by charge ordering of $Fe^{3+}$ and $Fe^{2+}$ ions and the symmetry lowering to the noncentrosymmetric monoclinic *Cc* symmetry. In the investigated film with a thikness of 55 nm, this transition occurs at a temperature of ~120 K, which is very close to the value for the bulk single crystal [2] and other magnetite thin films [24–27]. The Verwey transition around 120 K proves high quality and good stoichiometry of the film. The other feature is observed in the magnetization curves at a temperature of about 40 K and can be related to another transition, which can be accompanied, along with the magnetic moment variation, with the spontaneous electric polarization onset and susceptibility and permittivity peculiarities [6,7,28,29]. Ziesse et al. [7] showed that at this temperature magnetite transforms to the multiferroic phase.

The magnetite ferrimagnetic state is confirmed by the presence of hysteresis loops (Fig. 4). In addition, Fig. 4 shows two groups of dependences with different coercivities $H_C$, which are separated by the Verwey transition temperature $T_V$. Above this temperature, $H_C$ is about 300 Oe, and below this temperature, about 900 Oe. These values are higher than $H_C$ of the bulk single crystal, but typical of the epitaxial thin films [30,31]. The significant difference between

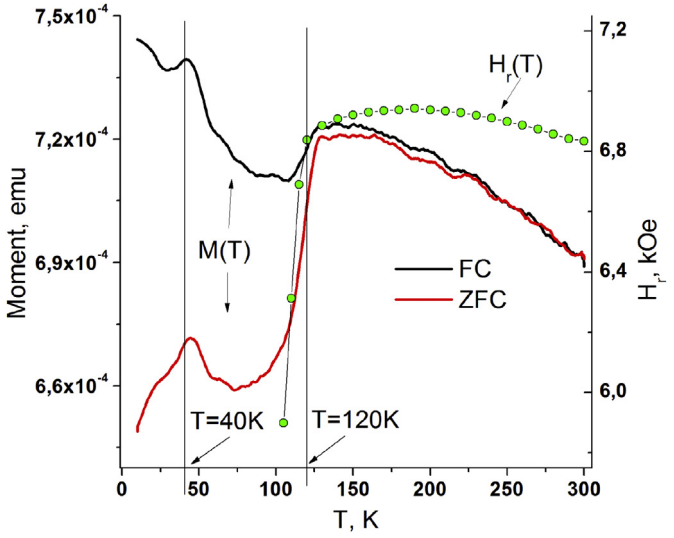


**Fig. 3.** FC and ZFC temperature dependences of magnetization in a magnetic field of 2 kOe (left axis). Temperature dependence of FMR out-of-plane resonance field (right axis).

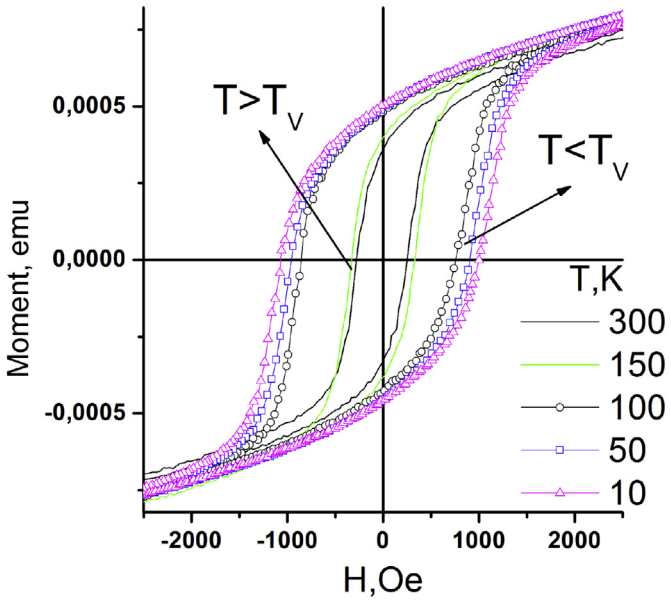


**Fig. 4.** Field dependences of magnetization for the $Fe_3O_4$/$SiO_2$/n-Si structure at different temperatures.

the $H_C$ values below and above $T_V$ is caused by the change in the magnetocrystalline anisotropy constants at the transition at 120 K [32,33]. We attempted to find these variations by measuring the angular dependences of the parameters of FMR spectra and analyzing their behavior (not shown here). The azimuthal dependences of FMR parameters were found to be isotropic. Comparative analysis of the polar dependences of the FMR parameters below and above $T_V$ showed no output of the easy magnetization axis from the plane. Possibly, the magnetocrystalline anisotropy variation was not directly observed because the films are textured and their orientation degree is only 30%. Nevertheless, the temperature dependence of out-of-plane resonance field $H_r$ agrees well with the M(T) behavior (Fig. 3).

### 3.3. Transport properties

Temperature dependences of resistivity $\rho$ were measured for four samples with thicknesses of 38, 46, 55, and 95 nm in the temperature range of 80–273 K (Fig. 5). At 300 K, resistivity ρ for the two thinner samples was about 25 mΩ cm; for the 55-nm-thick sample, 10 mΩ cm; and for the 102-nm-thick sample, 8 mΩ cm, which is somewhat higer than the resistivity ρ = 4 mΩ cm of the bulk $Fe_3O_4$ crystals [2]. An increase in the resistivity with decreasing thickness can be explained by a decrease in the grain size, especially in the crystallite width, and an increase in the number of grain boundaries with decreasing thickness. The obtained temperature dependences do not contain a sharp resistivity jump below $T_V$, which would be characteristic of single-crystal magnetite. Only a slight inflection in the ln(ρ) vs *1/T* curve can be observed in a narrow temperature range around $T_V$ (inset in Fig. 5). At the same time, over the entire temperature range the resistivity curves can be approximated by the equation of thermoactivated tunneling between nearest grains in a granular system [34].

$$\rho = \rho_0 \exp\left[2\left(\frac{C}{k_B}\right)^{1/2} T^{-1/2}\right], \quad (1)$$

where *C* is the activation energy and $k_B$ is the Boltzmann constant (Fig. 6). This equation describes carrier transport in granular systems and magnetite polycrystalline films [26,35,36].

Taking into account that the dependence of ln(ρ) on $(1/T)^{1/2}$ is linear and the resistivity does not sharply increases below 120 K, it would be reasonable to suggest that the dominant carrier transport mechanism is tunneling across the interface between two adjacent grains. In this case, the grain boundaries are possibly misoriented and electron tunneling occurs through the amorphous $Fe_3O_4$ phase.

Using Eq. (1), we extracted the fitting parameter $A = 2(C/k_B)^{1/2}$ and *C* for all the films and the entire temperature range of 80–273 K. In addition, using the Arrhenius law, we calculated the activation energy $E_a$ ($\rho = \rho_0 \exp(E_a/k_BT)$) for temperatures from 125 to 200 K. The approximation data are given in Table 1. Comparing the *C* and $E_a$ values, we can understand why we did not observe a sharp resistivity jump below $T_V$. The intergrain tunneling energy exceeds the polaron hopping energy by a factor of about 7 for all films thicknesses. As for the $E_a$ value, it is slightly higher than the values typical of the epitaxial films (50–70 meV [35,37]), which is no surprise, since our films are textured. In addition, as can be seen from Table 1, both the *C* and $E_a$ parameter decrease with increasing film thickness; for *C*, this occurs faster than for $E_a$. As in the case of the room-temperature resistivity, this behavior is consistent with the TEM data. Obviously, as the crystallite width is increased with increasing film thickness, the number of grain boundaries and, consequently, their contribution to the resistivity, decrease and both the intergrain tunneling energy and polaron hopping energy lower. The data on the transport properties show that the equivalent resistivity of grains is lower than the equivalent resistivity of the interface and, as a result, the features of the electrical properties of magnetite are barely observed.

### 3.4. Magnetotransport properties

To study magnetotransport properties of the films, we measured field dependences of MR at temperatures of 300 and 77 K (MR = 100% × [R(H) − R(0)]/R(0)) (Fig. 7). In our experiment,

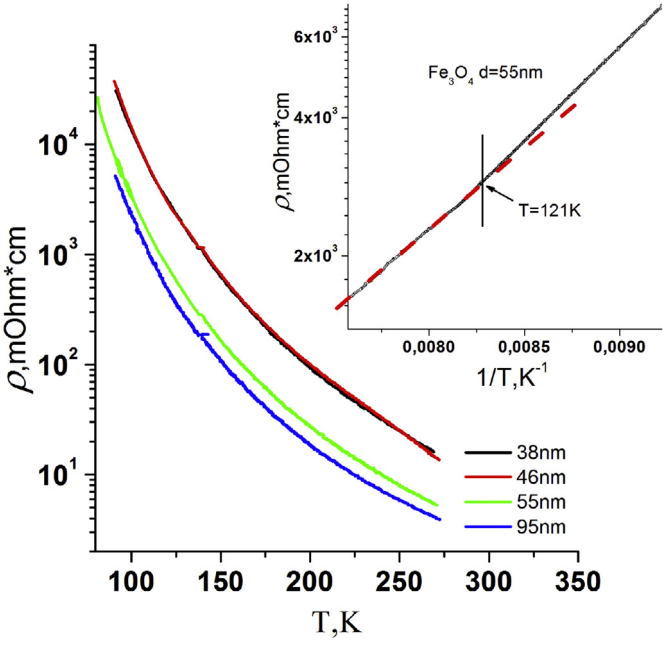


**Fig. 5.** Temperature dependences of resistivity of the magnetite films. Insert: ln(ρ) vs 1/T plot (solid line) with the linear fitting (dashed line).

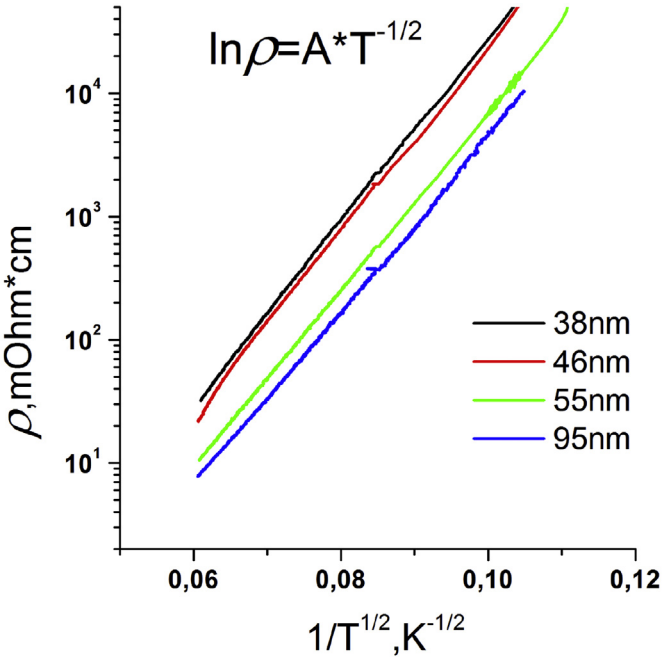


**Fig. 6.** ln(ρ) vs $1/T^{1/2}$ in the temperature range of 80–273 K.

**Table 1**
Fitting parameters.

| $d$, nm | $\ln(\rho) \sim \mathbf{A}\cdot(T^{-1/2})$ | $C$, eV | $\ln(\rho) \sim \mathbf{A}\cdot(T^{-1})$ | $E_a$, eV |
|---|---|---|---|---|
| 38 | 173.42 | 0.64788 | 1027 | 0.0885 |
| 46 | 170.77 | 0.62823 | 1006 | 0.0877 |
| 55 | 163.76 | 0.57771 | 976 | 0.0841 |
| 95 | 160.16 | 0.55259 | 940 | 0.0810 |

the magnetic field was applied in the (001) film plane parallel to the current (left inset of Fig. 7). For all film thicknesses, the field dependences behave qualitatively similarly. The quantitative difference is observed only for the thickest film in magnetic fields over 1 kOe. The maximum MR values were obtained for the 95-nm-thick film. The room-temperature MR of this sample in a field of 8 kOe is −1.6%. As the temperature is decreased below $T_V$, the MR value grows and attains −2.6%.

In magnetic fields below 2 kOe, the hysteresis and positive MR peak are observed in the MR curves (right-hand insert in Fig. 7). At temperatures below $T_V$, the MR peak shifts toward stronger fields in accordance with the coercivity growth in the hysteresis loops below $T_V$. The similar field dependences of MR were obtained for the epitaxial $Fe_3O_4$ films [15–17,38] and attributed, in particular, to the spin-dependent carrier transport across the AF APBs, which exists in both single crystals [39] and films [13,21,40]. In addition, taking into account the 30% degree of crystallite orientation and transport properties of the films, we should make allowance for the spin-dependent tunneling between grains. Then, the field dependences of MR can be described using the expression proposed in Ref. [15] for the $Fe_3O_4$ films

$$MR \sim \sum A_i (M/M_S)^{2i}, \quad (2)$$

where $M$ and $M_S$ are the magnetization and saturation magnetization, respectively and $A_i$ is the coefficient for different terms of the sum. We fitted the experimental data obtained for all the films at different temperatures to the data calculated using this equation. Fig. 8 shows that the experimental MR cruve is fitted well by the first two terms ($A_1 = -1.10$ and $A_2 = -0.35$) of Eq. (2). The use of

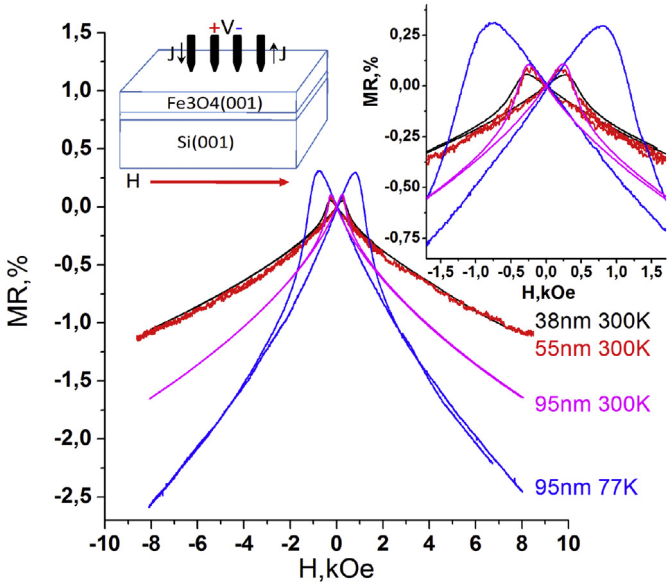


**Fig. 7.** Field dependences of MR for the magnetite films of different thicknesses at 300 and 77 K. Insert: the same dependences in weak magnetic fields.

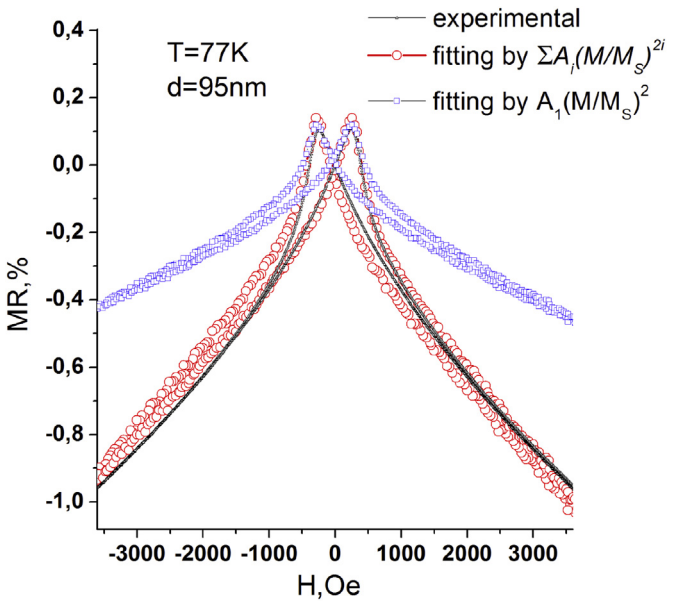


**Fig. 8.** Field dependence of MR for the magnetite films and approximation by Formula (2).

only the first term of the sum, which corresponds to MR of noninteracting granular systems, does not allow the observed dependences to be correctly described. Therefore, we may assume that the magnetotransport properties are determined not only by tunneling across grains, but also by tunneling across the AF APBs inside them. Matsuzaki et al. [38] obtained similar MR curves for annealed $Fe_3O_4$(111) epitaxial thin film, where the MR peaks appeared only below $T_V$. In our curves, this effect is observed over the entire temperature range. Recently, Dho et al. [17] reported the positive room-temperature MR in the (110) plane in weak fields. In Refs. [21], it was demonstrated using high-resolution TEM and density functional theory calculations that APB defects in the {110} planes are unusually stable and induce antiferromagnetic coupling between adjacent domains. Note that in our experiment the MR values were measured in the direction perpendicular to the {110} planes. In other words, spin-polarized electrons can face many AF APBs on their path. Thus, we can conclude that the observed MR effect is related to spin-dependent tunneling across $Fe_3O_4$ grains and antiferromagnetically coupled antiphase boundaries, the concentration of which in our $Fe_3O_4$ (001) textured films can be sufficiently high.

## 4. Conclusions

The structural, magnetic, and magnetotransport properties of $Fe_3O_4$ (001) thin films prepared by reactive deposition of Fe in the oxygen atmosphere were investigated. Analysis of the XRD data showed that the preferred orientation of the samples is (001) and their orientation degree is 30%. Using the cross-sectional TEM technique, we established that the crystallite height and width increase with film thickness. Temperature dependences of the magnetic moment have two features, one of them being observed at 120 K and attributed to the Verwey transition and the other, observed at 40 K and attributed to the ferroelectric phase [6]. The resistivity measurements of the samples with thicknesses of 38, 46, 55, and 95 nm in the temperature range of 80–273 K showed that the dominant carrier transport mechanism in the films is thermoactivated tunneling. The thermoactivation energy lowers with increasing film thickness, which can be caused by the crystallite

width variation. Meanwhile, the room-temperature resistivity of the 55- and 95-nm-thick films is similar to the value for the bulk crystals. At the same time, the specific shape of the field dependences of MR indicates that spin-dependent tunneling occurs across $Fe_3O_4$ grains and antiferromagnetically coupled antiphase boundaries. Thus, using reactive deposition of Fe in the oxygen atmosphere, we managed to obtain the high-quality films, which exhibit all the main properties typical of the epitaxial magnetite films. Nevertheless, the growth technology needs further improvement.

## Acknowledgments

This work was supported in part by the Russian Foundation for Basic Research, project no. 14-02-00234; the Russian Academy of Sciences, Program “Far East” no. 0262-2015-0057; and the Ministry of Education and Science of the Russian Federation, state order no. 16.663.2014K. The XRD study was supported by the state budget allocated to the Russian Academy of Sciences, fundamental research project no. V. 45.3.1. The authors are grateful to the Krasnoyarsk Regional Fund for Science and Technical Activity Support and the Council of the President of the Russian Federation on Grants.

## References

[1] E.J.W. Verwey, Nature 144 (1939) 327.
[2] F. Walz, J. Phys. Condens. Matter 14 (2002) R285.
[3] W. Mi, Z. Guo, Q. Wang, Y. Yang, H. Bai, Scr. Mater. 68 (2013) 972.
[4] M.S. Senn, J.P. Wright, J.P. Attfield, Nat. Lond. 481 (2012) 173.
[5] M.S. Senn, J.P. Wright, J. Cumby, J.P. Attfield, Phys. Rev. B 92 (2015) 024104.
[6] M. Alexe, M. Ziese, D. Hesse, P. Esquinazi, K. Yamauchi, T. Fukushima, S. Picozzi, U. Gosele, Adv. Mater 21 (2009) 4452.
[7] M. Ziese, P.D. Esquinazi, D. Pantel, M. Alexe, N.M. Nemes, M. Garcia-Hernandez, J. Phys. Condens. Matter 24 (2012) 086007.
[8] Z. Zhang, S. Satpathy, Phys. Rev. B44 (1991) 13319.
[9] M. Fonin, Yu S. Dedkov, R. Pentcheva, U. Rüdiger, G. Güntherodt, J. Phys. Condens. Matter 19 (2007) 315217.
[10] M. Ziese, Rep. Prog. Phys. 65 (2002) 143.
[11] H. Xiang, F. Shi, M.S. Rzchowski, P.M. Voyles, Y.A. Chang, Appl. Phys. Lett. 97 (2010) 092508.
[12] S.G. Bhat, P.S.A. Kumar, Sci. Rep. 4 (2014) 5588.
[13] W. Eerenstein, T. Palstra, T. Hibma, S. Celotto, Phys. Rev. B66 (2002) 201101.
[14] W.B. Mi, J.J. Shen, E.Y. Jiang, H.L. Bai, Acta Mater. 55 (2007) 1919.
[15] P. Li, L.T. Zhang, W.B. Mi, E.Y. Jiang, H.L. Bai, J. Appl. Phys. 106 (2009) 033908.
[16] O. Chichvarina, T.S. Herng, W. Xiao, X. Hong, J. Ding, J. Appl. Phys. 117 (2015) 17D722.
[17] J. Dho, B. Kim, S. Ki, J. Appl. Phys. 117 (2015) 163904.
[18] J.-B. Moussy, J. Phys. D. Appl. Phys. 46 (2013) 143001.
[19] W.B. Mi, E.Y. Jiang, H.L. Bai, J. Appl. Phys. 107 (2010) 103922.
[20] L.B. Zhao, W.B. Mi, E.Y. Jiang, H.L. Bai, Appl. Phys. Lett. 91 (2007) 052113.
[21] K.P. McKenna, F. Hofer, D. Gilks, V.K. Lazarov, C. Chen, Z. Wang, Y. Ikuhara, Nat. Commun. 5 (2014) 5740.
[22] L.A. Solovyov, J. Appl. Crystallogr. 37 (2004) 743.
[23] N.F.M. Henry, K. Lonsdale, Int. Tables X-Ray Crystallogr. 1 (1969) 340.
[24] R. Takahashi, H. Misumi, M. Lippmaa, J. Appl. Phys. 116 (2014) 033918.
[25] P. Li, Ch Jin, W.-B. Mi, H.-L. Bai, Chin. Phys. B 22 (2013) 047505.
[26] C. Jin, D.X. Zheng, P. Li, W.-B. Mi, H.-L. Bai, Appl. Surf. Sci. 287 (2013) 69–74.
[27] C. Boothman, A.M. Sánchez, S. van Dijken, J. Appl. Phys. 101 (2007) 123903.
[28] K. Dey, A. Ghosh, P. Modak, A. Indra, S. Majumdar, S. Giri, Appl. Phys. Lett. 105 (2014) 142905.
[29] G.T. Rado, J.M. Ferrari, Phys. Rev. B 12 (1975) 5166.
[30] G.Q. Gong, A. Gupta, G. Xiao, W. Qian, V.P. Dravid, Phys. Rev. B 56 (1997) 5096.
[31] R.G.S. Sofin, S.K. Arora, I.V. Shvets, Phys. Rev. B 83 (2011) 134436.
[32] L.R. Bickford, Rev. Mod. Phys. 25 (1953) 75.
[33] M.Y. Song, J.G. Lin, M.G. Samant, S.S.P. Parkin, IEEE Trans. Magn. 50 (11) (2014) 1002103.
[34] P. Sheng, B. Abeles, Y. Arie, Phys. Rev. Lett. 31 (1973) 44.
[35] R. Prakash, R.J. Choudhary, L.S. Sharath Chandra, N. Lakshmi, D.M. Phase, J. Phys. Condens. Matter 19 (2007) 486212.
[36] H. Liu, E.Y. Jiang, H.L. Bai, R.K. Zheng, X.X. Zhang, J. Phys. D. Appl. Phys. 36 (2003) 2950.
[37] S.B. Ogale, K. Ghosh, R.P. Sharma, R.L. Greene, R. Ramesh, T. Venkatesen, Phys. Rev. B 57 (1998) 7823.
[38] K. Matsuzaki, H. Hosono, T. Susaki, Appl. Phys. Express 6 (2013) 073009.
[39] D.T. Margulies, F.T. Parker, M.L. Rudee, F.E. Spada, J.N. Chapman, P.R. Aitchison, A.E. Berkowitz, Phys. Rev. Lett. (1997) 795162.
[40] D. Gilks, L. Lari, K. Matsuzaki, H. Hosono, T. Susaki, V.K. Lazarov, J. Appl. Phys. 115 (2014) 17C107.